Feedback Control Law of Solar Sail with Variable Surface Reflectivity at Sun-Earth Collinear Equilibrium Points

Lorenzo Niccolai*, Giovanni Mengali, Alessandro A. Quarta, Andrea Caruso

Department of Civil and Industrial Engineering, University of Pisa, I-56122 Pisa, Italy

Abstract

A solar sail generates thrust without consuming any propellant, so it constitutes a promising option for mission scenarios requiring a continuous propulsive acceleration, such as the maintenance of a (collinear) L_1-type artificial equilibrium point in the Sun-[Earth+Moon] circular restricted three-body problem. The usefulness of a spacecraft placed at such an artificial equilibrium point is in its capabilities of solar observation, as it guarantees a continuous monitoring of solar activity and is able to give an early warning in case of catastrophic solar flares. Because those vantage points are known to be intrinsically unstable, a suitable control system is necessary for station keeping purposes. This work discusses on how to stabilize an L_1-type artificial equilibrium point with a solar sail by suitably adjusting its lightness number and thrust vector orientation. A full-state feedback control law is assumed, where the control gains are chosen with a linear-quadratic regulator approach. In particular, the numerical simulation results show that an L_1-type artificial equilibrium point can be maintained with small required control torques, by using a set of reflectivity control devices.

Keywords: Solar sail, artificial equilibrium point, Sun's observation mission, reflectivity control

Nomenclature

A	=	total sail area, m^2
$\mathbb{A}$, $\widetilde{\mathbb{A}}$, $\mathbb{B}$, $\mathbb{B}_v$, $\mathbb{C}$	=	auxiliary matrices
$\boldsymbol{a}$	=	dimensionless propulsive acceleration vector
B	=	non-Lambertian coefficient
$\{b_1, b_2, b_3\}$	=	dimensionless optical parameters, see Eqs. (4)
C	=	center-of-mass
$\{c_1, c_2, c_3\}$	=	dimensionless constants, see Eqs. (18)
G	=	universal gravitational constant, $\mathrm{N\,m^2/kg^2}$
I	=	principal moment of inertia, $\mathrm{kg\,m^2}$
$\mathbb{I}$	=	identity matrix
J	=	LQR functional, see Eq. (29)
$\mathbb{K} \triangleq [\mathbb{K}_p \, \mathbb{K}_d]$	=	control gain matrix
k_{pi}, k_{di}	=	proportional and derivative gains ($i = 1, \ldots 3$)
l	=	Sun-[Earth+Moon] distance, au
M	=	control torque component, $\mathrm{N\,m}$
m	=	mass, kg
$\hat{\boldsymbol{n}}$	=	sail normal unit vector
$\mathbb{O}$	=	zero matrix

*Corresponding author

Email addresses: lorenzo.niccolai@ing.unipi.it (Lorenzo Niccolai), g.mengali@ing.unipi.it (Giovanni Mengali), a.quarta@ing.unipi.it (Alessandro A. Quarta), andrea.caruso@ing.unipi.it (Andrea Caruso)

Published in Aerospace Science and Technology, Vol. 106, November 2020, pp. 106144 (1–13). doi: https://doi.org/10.1016/j.ast.2020.106144

P	=	solar radiation pressure, μ Pa
$\mathbb{Q}_x$, $\mathbb{Q}_u$	=	weighting matrices
$\mathbb{R}$	=	rotational matrix
$\boldsymbol{r}$	=	dimensionless position vector
$\widetilde{r}$	=	reflectivity coefficient
S	=	spacecraft center-of-mass
$\boldsymbol{T}$	=	solar sail thrust vector, N
$\mathcal{T}(C;\hat{\boldsymbol{\imath}},\hat{\boldsymbol{\jmath}},\hat{\boldsymbol{k}})$	=	synodic reference frame
$\mathcal{T}_b(S;\hat{\boldsymbol{n}},\hat{\boldsymbol{p}},\hat{\boldsymbol{q}})$	=	body reference frame
t	=	time, years
$\boldsymbol{u}$	=	control vector
$\delta\dot{\boldsymbol{r}} \triangleq [v_x,\ v_y,\ v_z]^{\mathrm{T}}$	=	dimensionless velocity perturbation
$\boldsymbol{x}$	=	state vector
$\delta\boldsymbol{r} \triangleq [x,\ y,\ z]^{\mathrm{T}}$	=	dimensionless position perturbation
β	=	sail lightness number
$\delta\beta$	=	lightness number variation
ϵ	=	emissivity coefficient
$\{\theta,\ \psi\}$	=	Euler angles, rad
$\lambda_i\ (i = 1, \dots 6)$	=	eigenvalue of matrix $\widetilde{\mathbb{A}}$
μ	=	[Earth+Moon]'s dimensionless mass
$\bar{\mu}$	=	auxiliary constant, see Eq. (19)
$\boldsymbol{\rho}$	=	dimensionless primary-spacecraft vector (with $\rho \triangleq \|\boldsymbol{\rho}\|$)
σ	=	solar sail areal density, g/m^2
$\boldsymbol{\omega}$	=	spacecraft angular velocity w.r.t. an inertial frame, rad/s

Subscripts

$\odot$	=	Sun
$\oplus$	=	[Earth+Moon]
0	=	initial value
$\{1, 2, 3\}$	=	body-frame components
b	=	back sail surface
e	=	equilibrium value
f	=	front sail surface
S	=	spacecraft

Superscripts

$\cdot$	=	dimensionless time derivative
T	=	transpose
$\wedge$	=	unit vector

1. Introduction

The features of the circular restricted three-body problem (CR3BP) [1, 2] allow transfer trajectories with small propellant consumption to be designed by exploiting the existence of invariant manifolds, as is discussed in Refs. [3, 4, 5, 6] in the case of the Earth-Moon CR3BP. A potential application of the results of the CR3BP analysis is constituted by space missions orbiting around equilibrium points. In particular,

the Sun-Earth collinear L_1 point is located along the Sun-Earth direction at about 1.5 million kilometers from Earth, and a spacecraft (or a constellation [7, 8]) placed there is able both to perform a continuous solar observation, and to guarantee an early warning in case of catastrophic solar events. Currently, NASA's Advanced Composition Explorer (ACE) is monitoring the solar activity while tracking a Lissajous orbit around the Sun-Earth L_1 point, which guarantees an early warning time of about 1 hour [9]. In principle, such a warning time could be further increased by means of propellantless propulsion systems such as solar sails or electric solar wind sails [10, 11, 12], which are able to artificially displace the collinear point towards the Sun by exploiting a continuous (outward) radial thrust. In this regard, the Authors [13] have recently analyzed the impact of solar wind fluctuations [14] on the dynamics of an electric solar wind sail orbiting around the Sun-Earth L_1 point. In particular, Ref. [13] proposes a simplified control law that exploits a suitable variation of tether electric voltage to counteract the fluctuations of the solar wind characteristics and to stabilize the spacecraft motion around such an equilibrium point. However, this sort of "voltage-control" is peculiar to the electric solar wind sail and cannot be employed in case of solar sails.

The potentiality of solar sails in envisaging advanced mission scenarios have been extensively discussed in the literature, with several works proposing solar sail-based phasing maneuvers [15], non-Keplerian orbits [16], scientific observation of Earth's magnetosphere [17], near-Earth asteroid exploration [18], and transfers to Lagrangian points [19]. The use of solar sails to generate collinear artificial equilibrium points (AEPs) must face the intrinsic instability of such equilibrium positions. This implies that a station keeping is possible only provided the spacecraft is equipped with a suitable control system. In this regard, some possible choices are available for a solar sail-based spacecraft. For example, cold gas thrusters or momentum wheels could in principle be used as actuation means, although their large mass would decrease the sail performance. A more promising alternative is offered by electrochromic materials [20, 21], which are able to modify their reflectivity upon application of a low electric voltage. Electrochromic materials allow the manufacturing of reflectivity control devices (RCDs), which may be used to adjust the sail thrust, as discussed in Refs. [17, 22]. Moreover, RCDs can also generate control torques belonging to the sail plane, which are useful to properly orient the propulsive acceleration vector, as tested (and validated) by the pioneering IKAROS mission [23]. The flexibility of RCDs could be further increased by means of polymer dispersed liquid crystals (PDLCs) [24, 25], which may refract the incoming sunlight to generate a small tangential force, and so a control torque perpendicular to the sail nominal plane. A further strategy for varying the sail thrust magnitude and direction has been recently discussed by Luo et al. [26], who proposed the concept of a solar sail composed of controllable blade elements. The relative rotation of such blades, generated by electric actuators, is able to change the sail attitude and also to slightly adjust the thrust vector direction and magnitude.

The idea of generating AEPs with a solar sail is not new, and, in fact, such a problem has been addressed in the literature from different viewpoints, including the maintenance of AEPs [22, 27, 28, 29, 30], or the generation of periodic orbits around AEPs [31, 32]. In particular, the AEP maintenance scenario may be viewed as a case useful for quantifying the upper performance bounds for a given solar sail-based spacecraft. Actually, a more realistic scientific mission would not require the vehicle to be constantly placed at the AEP, as this is not the best choice for guaranteeing a good tracking and communication with the ground station. However, a solution to the communication problem may be obtained by allowing the sail to librate at a certain distance from the Ecliptic plane.

The existing studies on AEPs maintained by solar sails are based on simplifying assumptions, such as that of an ideal (i.e., perfectly reflecting) sail or a constant sail attitude, and, more importantly, do not give any estimation of the control torques necessary to meet the mission requirements. The aim of this work is to fill that gap with a preliminary analysis of the maintenance problem of an L_1-type AEP in the Sun-Earth CR3BP using a solar sail with RCD-based control systems, which are assumed to be able to modify both the sail lightness number and the sail attitude. The sail thrust is here modelled with an optical force model, using the recent results obtained by NASA during the preliminary phase of NEA Scout mission [33]. A full-state feedback control system is used to compensate for the dynamics instability, where the control gains are chosen with a linear-quadratic regulator approach. The actual performance of the control law is evaluated via numerical simulations, and the required control torques are estimated by means of Euler's equations, in order to assess the feasibility of the mission scenario maintenance. The obtained results show that a simplification of the control system is possible, with a negligible decrease of the performance level defined in terms of early warning time for a solar observation mission.

2. Mathematical model

Assume that a solar sail-based spacecraft S is moving under the gravitational forces exerted by the Sun and the [Earth+Moon], where [Earth+Moon] denotes the position of the center of mass of the Earth-Moon system. The analysis of the orbital motion of S can be simplified by means of two fundamental assumptions of the CR3BP [1] . First, the spacecraft mass m_S is considered negligible with respect to the Sun's mass $m_\odot$ and the [Earth+Moon]'s mass $m_\oplus$, so that the motion of the primaries is unaffected by the presence of the spacecraft. In the second place, the orbital eccentricity of the primaries is neglected, so that they are assumed to track two coplanar circular orbits around the center-of-mass of the system C. Accordingly, the Sun and the [Earth+Moon] maintain a constant relative distance $l \triangleq 1\,\text{au}$.

Introduce a Cartesian synodic reference frame $\mathcal{T}(C;\hat{\boldsymbol{\imath}},\hat{\boldsymbol{\jmath}},\hat{\boldsymbol{k}})$, which rotates with respect to an inertial frame with a constant angular velocity of magnitude $\omega_\oplus \triangleq \sqrt{G(m_\oplus + m_\odot)/l^3} = 2\pi\,\text{rad/year}$, where G is the universal gravitational constant. The unit vector $\hat{\boldsymbol{\imath}}$ points from the Sun to the [Earth+Moon], and $\hat{\boldsymbol{k}}$ is perpendicular to the ecliptic plane in the direction of the angular momentum vector; see Fig. 1. Using the

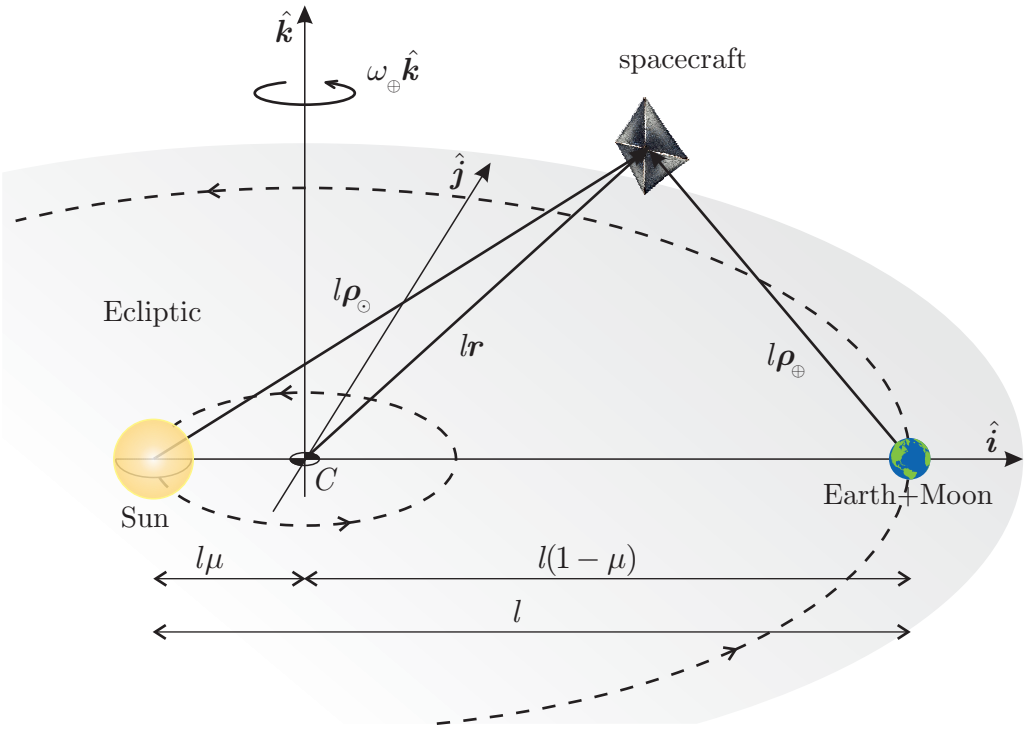

Figure 1: Sketch of the Sun-[Earth+Moon] CR3BP framework. Adapted from Ref. [34].

standard notation of CR3BP [1], the total mass $(m_\odot + m_\oplus)$ of the two primaries is taken as the reference mass, and the (constant) distance l is chosen as the reference length. Finally, the time t is expressed in dimensionless units by normalizing $\omega_\oplus$ to 1. Accordingly, the [Earth+Moon] dimensionless mass is $\mu \triangleq m_\oplus/(m_\odot + m_\oplus) \simeq 3.0404 \times 10^{-6}$ [2] , while the dimensionless distance between C and the [Earth+Moon] (or the Sun) is $1-\mu$ (or μ), as shown in Fig. 1.

Bearing in mind that the angular velocity vector of the rotating reference frame can be expressed as $\hat{\boldsymbol{k}}$ in dimensionless units, the motion of S is described by the following differential equation [35]

$$\ddot{\boldsymbol{r}} + 2\,\hat{\boldsymbol{k}} \times \dot{\boldsymbol{r}} + \hat{\boldsymbol{k}} \times \left(\hat{\boldsymbol{k}} \times \boldsymbol{r}\right) + \frac{1-\mu}{\rho_\odot^3}\,\boldsymbol{\rho}_\odot + \frac{\mu}{\rho_\oplus^3}\,\boldsymbol{\rho}_\oplus = \boldsymbol{a} \tag{1}$$

where the dot symbol denotes a derivative with respect to the dimensionless time $(t\,\omega_\oplus)$, $\boldsymbol{a}$ denotes the dimensionless propulsive acceleration vector provided by the solar sail, while $\boldsymbol{r}$, $\boldsymbol{\rho}_\odot$ and $\boldsymbol{\rho}_\oplus$ are the dimensionless

position vectors of S with respect to C, the Sun, and the [Earth+Moon], respectively, with $\rho_\odot \triangleq \left\|\boldsymbol{\rho}_\odot\right\|$ and $\rho_\oplus \triangleq \left\|\boldsymbol{\rho}_\oplus\right\|$. By geometrical considerations, it is possible to express the vectors $\boldsymbol{r}$ and $\boldsymbol{\rho}_\oplus$ as

$$\boldsymbol{r} = \boldsymbol{\rho}_\odot - \mu\,\hat{\boldsymbol{i}} \quad , \qquad \boldsymbol{\rho}_\oplus = \boldsymbol{r} - (1-\mu)\hat{\boldsymbol{i}} = \boldsymbol{\rho}_\odot - \hat{\boldsymbol{i}} \tag{2}$$

which allows Eq. (1) to be rewritten more conveniently as

$$\ddot{\boldsymbol{\rho}}_\odot + 2\,\hat{\boldsymbol{k}} \times \dot{\boldsymbol{\rho}}_\odot + \hat{\boldsymbol{k}} \times \left[\hat{\boldsymbol{k}} \times \left(\boldsymbol{\rho}_\odot - \mu\,\hat{\boldsymbol{i}}\right)\right] + \frac{1-\mu}{\rho_\odot^3}\,\boldsymbol{\rho}_\odot + \frac{\mu}{\left\|\boldsymbol{\rho}_\odot - \hat{\boldsymbol{i}}\right\|^3}\,\left(\boldsymbol{\rho}_\odot - \hat{\boldsymbol{i}}\right) = \boldsymbol{a} \tag{3}$$

Therefore, the spacecraft dynamics can be analyzed once the propulsive acceleration vector $\boldsymbol{a}$ is described by a suitable solar sail thrust model.

2.1. Solar sail thrust model and propulsive acceleration expression

Several mathematical models have been proposed in the literature to express the thrust generated by a flat solar sail. Among them, the ideal force model [36, 37] is the first and simpler one, as it assumes that each photon incident on the sail surface is specularly reflected. This assumption provides a handy and analytical expression for the sail thrust, but it leads to oversimplified and non-conservative results. In the following analysis an optical force model is used, which takes into account the optical properties of the sail film [36, 37, 38] and represents a good compromise between simplicity and accuracy. Other (more complex) sail thrust models take into account the sail billowing effect [39], the sail film's optical degradation with time [40, 41], the fluctuations of solar radiation pressure [42], or the light polarization and the sail surface roughness [43, 44], which are all neglected by the optical model. Finally, it is assumed that the sail attitude is known at each time instant, without orientation uncertainties. In this context, the thrust vector $\boldsymbol{T}$ generated by a solar sail-based spacecraft may be written as [37]

$$\boldsymbol{T} = \frac{2\,P_\oplus\,A}{\rho_\odot^2}\,\frac{\hat{\boldsymbol{\rho}}_\odot \cdot \hat{\boldsymbol{n}}}{b_1 + b_2 + b_3}\,\left\{b_1\,\hat{\boldsymbol{\rho}}_\odot + \left[b_2\,(\hat{\boldsymbol{\rho}}_\odot \cdot \hat{\boldsymbol{n}}) + b_3\right]\hat{\boldsymbol{n}}\right\} \tag{4}$$

where $P_\oplus \triangleq 4.563\,\mu\,\mathrm{Pa}$ is the solar radiation pressure at a Sun-[Earth+Moon] distance, A is the sail reflective area, $\hat{\boldsymbol{\rho}}_\odot \triangleq \boldsymbol{\rho}_\odot/\rho_\odot$ is the Sun-spacecraft unit vector, and $\hat{\boldsymbol{n}}$ is the unit vector normal to the sail nominal surface in the direction opposite to the Sun. In Eq. (4), the dimensionless parameters $\{b_1,\, b_2,\, b_3\}$ are related to the optical characteristics of the sail film material, viz.

$$b_1 = \frac{1 - \widetilde{r}\,s}{2} \quad , \quad b_2 = \widetilde{r}\,s \quad , \quad b_3 = \frac{B_f\,\widetilde{r}\,(1-s)}{2} + \frac{(1-\widetilde{r})\,(\epsilon_f\,B_f - \epsilon_b\,B_b)}{2\,(\epsilon_f + \epsilon_b)} \tag{5}$$

where $\widetilde{r}$ is the reflectivity coefficient, s is the fraction of specularly reflected photons, B_f (or B_b) is the front (or back) non-Lambertian coefficient, and ϵ_f (or ϵ_b) is the front (or back) sail surface emissivity.

The optical characteristics involved in the calculation of $\{b_1,\, b_2,\, b_3\}$ have been recently estimated by experimental measurements and numerical simulations performed by NASA [45, 46] during the preliminary phase of NEA Scout mission, yielding

$$\widetilde{r} = 0.91 \quad , \quad s = 0.89 \quad , \quad B_f = 0.79 \quad , \quad B_b = 0.67 \quad , \quad \epsilon_f = 0.025 \quad , \quad \epsilon_b = 0.27 \tag{6}$$

Accordingly, the values of the parameters in Eq. (4) are

$$b_1 = 0.0950 \quad , \quad b_2 = 0.8099 \quad , \quad b_3 = 0.0150 \tag{7}$$

Note that the b_3 term gives a small contribution, as confirmed by authors' previous work [47].

From Eq. (4), it is possible to calculate the dimensionless acceleration vector $\boldsymbol{a}$ to be substituted into Eq. (1). Let β be the solar sail lightness number [37], that is, the performance parameter defined as the ratio of the propulsive acceleration generated in a Sun-facing configuration to the Sun's local gravitational attraction at a given heliocentric distance. With the standard CR3BP notation, the propulsive acceleration vector $\boldsymbol{a}$ can therefore be written as

$$\boldsymbol{a} = \beta\,\frac{1-\mu}{\rho_\odot^2}\,(\hat{\boldsymbol{\rho}}_\odot \cdot \hat{\boldsymbol{n}})\,\frac{1}{b_1 + b_2 + b_3}\,\left\{b_1\,\hat{\boldsymbol{\rho}}_\odot + \left[b_2\,(\hat{\boldsymbol{\rho}}_\odot \cdot \hat{\boldsymbol{n}}) + b_3\right]\hat{\boldsymbol{n}}\right\} \tag{8}$$

2.2. Reference mission scenario and spacecraft linearized dynamics

In our reference mission scenario, a solar sail-based spacecraft is placed at a collinear L_1-type AEP. The continuous propulsive acceleration is used to displace the natural L_1 (collinear) point towards the Sun, as is illustrated in Fig. 2. Note that the Sun-sail distance is characterized by the subscript e, which is used here to denote the nominal (reference) equilibrium point.

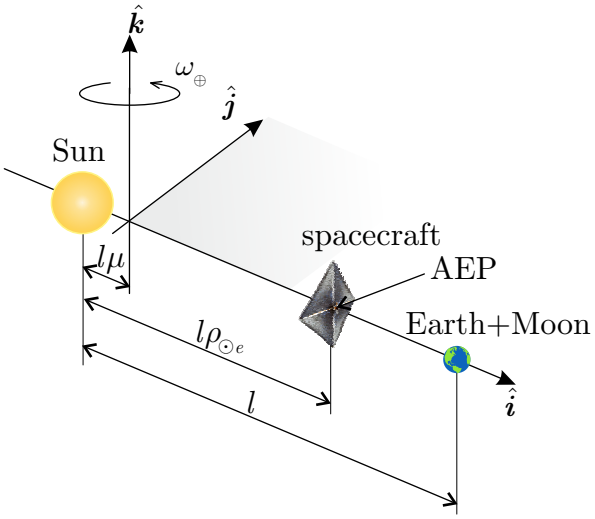

Figure 2: Sketch of a collinear L_1-type AEP.

The location of an L_1-type AEP in the CR3BP system may be found by substituting Eqs. (2) and (8) into Eq. (1), and by imposing the first and second derivatives of the position vector to be zero. Because such an L_1-type AEP lies on the line connecting the two primaries, its dimensionless position and velocity vectors are given by

$$\boldsymbol{r}_e = [\rho_{\odot_e} - \mu,\ 0,\ 0]^{\mathrm{T}} \qquad \dot{\boldsymbol{r}}_e = [0,\ 0,\ 0]^{\mathrm{T}} \tag{9}$$

and the required propulsive acceleration $\boldsymbol{a}_e$ is aligned along the $\hat{\boldsymbol{i}}$-direction, viz.

$$\boldsymbol{a}_e = \beta_e \frac{1-\mu}{\rho_{\odot_e}^2}\hat{\boldsymbol{i}} \tag{10}$$

so that the only nonzero component of Eq. (1) is

$$-\rho_{\odot_e} + \mu + \frac{1-\mu}{\rho_{\odot_e}^2} - \frac{\mu}{(1-\rho_{\odot_e})^2} = \beta_e \frac{1-\mu}{\rho_{\odot_e}^2} \tag{11}$$

which gives

$$\beta_e = 1 - \frac{\mu\,\rho_{\odot_e}^2}{1-\mu}\left[\frac{\rho_{\odot_e}}{\mu} + \frac{1}{(1-\rho_{\odot_e}^2)} - 1\right] \tag{12}$$

From the last equation, the equilibrium distance $\rho_{\odot_e}$ may be easily found numerically as a function of a given (reference) sail lightness number β_e.

To study the dynamical behavior of a solar sail-based spacecraft in the vicinity of an L_1-type AEP, use the transformation

$$\boldsymbol{r} = \boldsymbol{r}_e + \delta\boldsymbol{r} \triangleq [\rho_{\odot_e} - \mu + x,\ y,\ z]^{\mathrm{T}} \qquad \dot{\boldsymbol{r}} \equiv \delta\dot{\boldsymbol{r}} \triangleq [v_x,\ v_y,\ v_z]^{\mathrm{T}} \tag{13}$$

where $\{x,\ y,\ z\} \ll 1$ and $\{v_x,\ v_y,\ v_z\} \ll 1$ are considered as perturbation terms, and introduce the state vector $\boldsymbol{x}$ defined as

$$\boldsymbol{x} \triangleq [\delta\boldsymbol{r}^{\mathrm{T}},\ \delta\dot{\boldsymbol{r}}^{\mathrm{T}}]^{\mathrm{T}} = [x,\ y,\ z,\ v_x,\ v_y,\ v_z]^{\mathrm{T}} \tag{14}$$

of which the components are the position and velocity errors relative to the L_1-type AEP; see Eqs. (9). Substituting Eqs. (13) into Eq. (1), subtracting the equilibrium solution given by Eq. (11) and neglecting the second-order perturbation terms, the spacecraft linearized dynamics may be written in a compact form as

$$\dot{\boldsymbol{x}} = \mathbb{A}\,\boldsymbol{x} \tag{15}$$

where

$$\mathbb{A} = \begin{bmatrix} \mathbb{O} & \mathbb{I} \\ \mathbb{C} & \mathbb{D} \end{bmatrix} \tag{16}$$

in which $\mathbb{O}$ is a 3×3 zero matrix, $\mathbb{I}$ is a 3×3 identity matrix, while matrices $\mathbb{C}$ and $\mathbb{D}$ are defined as

$$\mathbb{C} \triangleq \begin{bmatrix} c_1 & 0 & 0 \\ 0 & c_2 & 0 \\ 0 & 0 & c_3 \end{bmatrix}, \qquad \mathbb{D} \triangleq \begin{bmatrix} 0 & 2 & 0 \\ -2 & 0 & 0 \\ 0 & 0 & 0 \end{bmatrix} \tag{17}$$

with

$$c_1 \triangleq 1 + 2\bar{\mu} - 2\,\beta_e \frac{1-\mu}{\rho_{\odot_e}^3}, \qquad c_2 \triangleq 1 - \bar{\mu}, \qquad c_3 \triangleq -\bar{\mu} \tag{18}$$

where, in analogy with Ref. [2], the constant $\bar{\mu} > 0$ is written as

$$\bar{\mu} \triangleq \frac{\mu}{(1-\rho_{\odot_e})^3} + \frac{1-\mu}{\rho_{\odot_e}^3} \tag{19}$$

A collinear L_1-type AEP is unstable [29, 48], as is confirmed by one positive eigenvalue of matrix $\mathbb{A}$ in Eq. (16). Therefore, to guarantee the AEP maintenance, the spacecraft must be equipped with a suitable control system.

3. Feedback control law for equilibrium point maintenance

In this study, it is assumed that the solar sail is capable of modifying both the magnitude and the direction of the propulsive acceleration $\boldsymbol{a}$, and that these modifications can be actuated independently. This is possible by exploiting the properties of electrochromic materials and making use of RCDs located on the sail surface. In fact, the activation (or deactivation) of electrochromic actuators increases (or decreases) the thrust generated by the fraction of sail area covered by the RCD, as sketched in Fig. 3. In analogy with previous works [17], it is assumed that such variation is continuous, which amounts to stating that the sail is equipped with a large number of small RCDs.

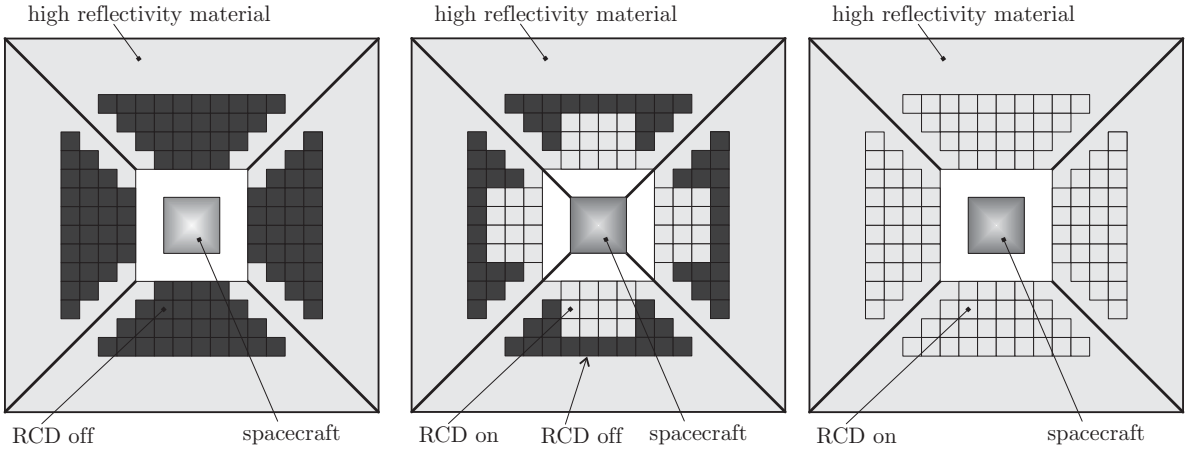

(a) Minimum thrust. (b) Intermediate thrust. (c) Maximum thrust.

Figure 3: Basic sketch of thrust control by means of RCDs. Adapted from Ref. [49].

In particular, RCDs could be also used to generate control torques capable of modifying the sail attitude, that is, varying the direction of the sail normal $\hat{\boldsymbol{n}}$ and therefore the direction of the propulsive acceleration vector; see Eq. (8). A conceptual sketch of an attitude control system based on RCDs is given in Fig. 4, which shows that control torques lying on the sail nominal plane are obtainable with RCDs, whereas a control torque normal to the sail nominal plane (i.e., along the direction of $\hat{\boldsymbol{n}}$) must be generated with a different strategy. To that end, a promising option is the utilization of PDLCs [24, 25], which are capable of exploiting the incident photons to generate a tangential force.

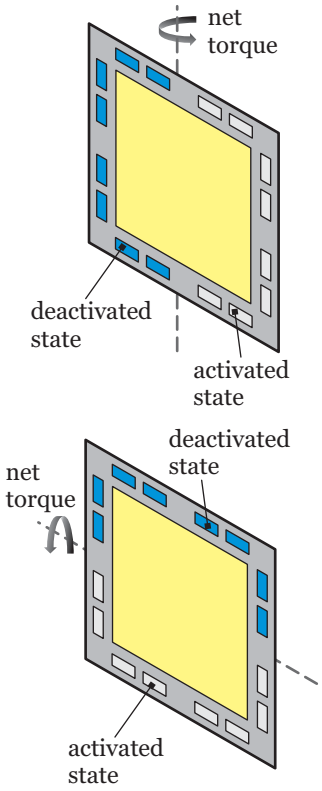

Figure 4: Sketch of RCD-based attitude control system.

To describe the solar sail attitude, which determines the direction of $\boldsymbol{a}$, it is useful to introduce a body reference frame $\mathcal{T}_b(S;\hat{\boldsymbol{n}},\hat{\boldsymbol{p}},\hat{\boldsymbol{q}})$ with origin at the spacecraft center-of-mass, whose unit vectors $\{\hat{\boldsymbol{p}},\,\hat{\boldsymbol{q}}\}$ lie on the sail nominal plane along the principal axes of inertia; see Fig. 5. Note that when the spacecraft is at its design L_1-type AEP, $\hat{\boldsymbol{p}}$ lies on the ecliptic plane, while $\hat{\boldsymbol{q}}$ is perpendicular to it. Two consecutive rotations, of angles θ and ψ, are required to superimpose the axes of the synodic frame $\mathcal{T}$ to those of the body frame $\mathcal{T}_b$; see Fig. 6. Accordingly, the rotation matrix from $\mathcal{T}$ to $\mathcal{T}_b$ is

$$\mathbb{R} = \mathbb{R}_2(\theta)\,\mathbb{R}_3(\psi) = \begin{bmatrix} \cos\theta\,\cos\psi & \sin\psi\,\cos\theta & -\sin\theta \\ -\sin\psi & \cos\psi & 0 \\ \cos\psi\,\sin\theta & \sin\psi\,\sin\theta & \cos\theta \end{bmatrix} \tag{20}$$

where $\mathbb{R}_2$ and $\mathbb{R}_2$ are the principal rotations about the 2- or 3-axis, respectively [50].

A third Euler angle would be required to describe the sail rotation around the direction of $\hat{\boldsymbol{n}}$, which however does not affect the orientation of the propulsive acceleration vector $\boldsymbol{a}$ and, therefore, is neglected in the following analysis. Note that the components of $\hat{\boldsymbol{n}}$ in the synodic frame are

$$[\hat{\boldsymbol{n}}]_{\mathcal{T}} = \mathbb{R}^{\mathrm{T}}\,[1 \quad 0 \quad 0]^{\mathrm{T}} = [\cos\theta\,\cos\psi \qquad \sin\psi\,\cos\theta \qquad -\sin\theta]^{\mathrm{T}} \tag{21}$$

When Eq. (21) is substituted into Eq. (8), the components of the propulsive acceleration in $\mathcal{T}$ are obtained

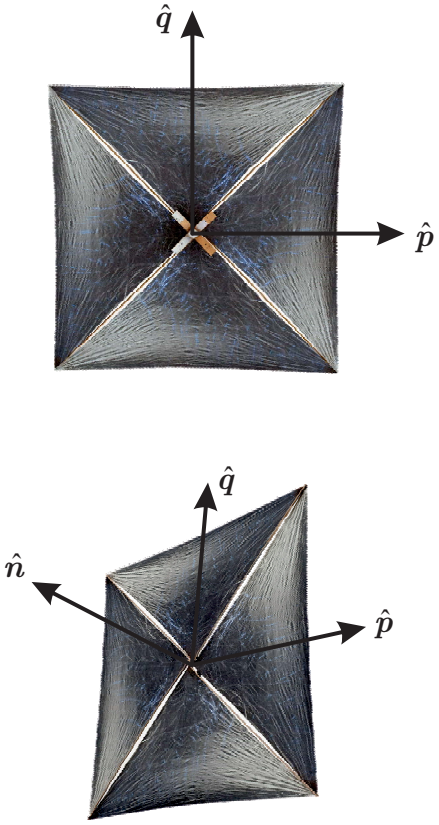

Figure 5: Orientation of the unit vectors of body-fixed reference frame $\mathcal{T}_b(S;\hat{\boldsymbol{n}},\hat{\boldsymbol{p}},\hat{\boldsymbol{q}})$.

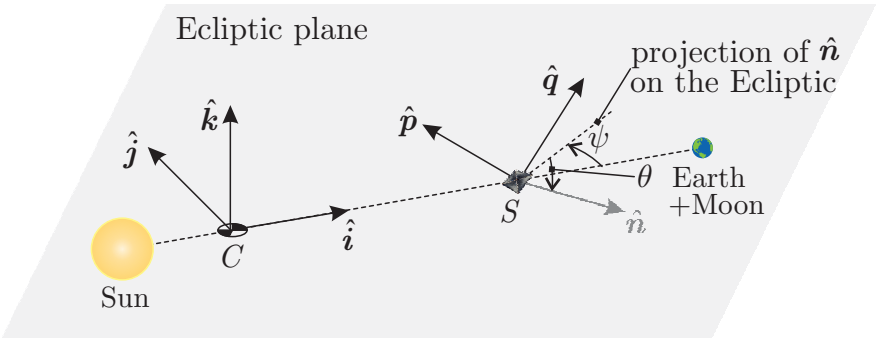

Figure 6: Mutual orientation of $\mathcal{T}$ and $\mathcal{T}_b$ and Euler angles definition.

as

$$[\boldsymbol{a}]_{\mathcal{T}} = \beta\,\frac{1-\mu}{\rho_{\odot}^{2}}\,\cos\psi\,\cos\theta\,\frac{1}{b_1+b_2+b_3}\begin{bmatrix} b_1+b_2\cos^2\psi\,\cos^2\theta+b_3\cos\psi\,\cos\theta \\ \cos\theta\,\sin\psi\,(b_2\,\cos\theta\,\cos\psi+b_3) \\ -\sin\theta\,(b_2\cos\psi\,\cos\theta+b_3)\end{bmatrix} \tag{22}$$

Recall that in an equilibrium condition at the L_1-type AEP, the sail is in a Sun-facing configuration, that is, $\psi=\theta=0$ and $\beta=\beta_e$.

The solar sail is controlled by means of a (small) variation of the lightness number $\delta\beta \triangleq \beta-\beta_e$ and through a suitable orientation of the propulsive acceleration vector, which is defined by the Euler angles ψ and θ. As a result, the (dimensionless) control vector is given by

$$\boldsymbol{u} \triangleq [\delta\beta,\ \psi,\ \theta]^{\mathrm{T}} \tag{23}$$

where ψ and θ have to be regarded as virtual inputs in that they may be generated by means of suitable torques, as will be discussed later. Equation (22) may be simplified under the assumption of small Euler angles, that is, by considering $\cos\psi \simeq 1$, $\cos\theta \simeq 1$, $\sin\psi \simeq \psi$, and $\sin\theta \simeq \theta$. Likewise, the inverse squared Sun-spacecraft distance is $\rho_{\odot}^{-2} = [(\rho_{\odot_e} + x)^2 + y^2 + z^2]^{-1} \simeq \rho_{\odot_e}^{-2}(1 - 2\,x/\rho_{\odot_e})$, so that Eq. (22) becomes

$$[\boldsymbol{a}]_{\mathcal{T}} = (\beta_e + \delta\beta)\,\frac{1-\mu}{\rho_{\odot_e}^2}\left(1 - \frac{2\,x}{\rho_{\odot_e}}\right)\begin{bmatrix} 1 \\ \psi\,\dfrac{b_2+b_3}{b_1+b_2+b_3} \\ -\theta\,\dfrac{b_2+b_3}{b_1+b_2+b_3} \end{bmatrix} \tag{24}$$

where the minus sign in the last row comes from the definition of θ, which is positive when the unit vector $\hat{\boldsymbol{n}}$ points below the ecliptic plane.

The (linearized) spacecraft dynamics around the design L_1-type AEP is obtained by substituting Eq. (24) into Eq. (1), subtracting the equilibrium condition (10), and neglecting the second order terms. The resulting dynamical equations in the vicinity of an L_1-type point are in the form

$$\dot{\boldsymbol{x}} = \mathbb{A}\boldsymbol{x} + \mathbb{B}\boldsymbol{u} \tag{25}$$

where $\boldsymbol{x}$ and $\mathbb{A}$ are given by Eqs. (14) and (16), respectively, the control vector $\boldsymbol{u}$ is defined in Eq. (23), and

$$\mathbb{B} = \begin{bmatrix} \mathbb{O} \\ \mathbb{B}_v \end{bmatrix} \tag{26}$$

with

$$\mathbb{B}_v \triangleq \frac{1-\mu}{\rho_{\odot_e}^2}\begin{bmatrix} 1 & 0 & 0 \\ 0 & \beta_e\,\dfrac{b_2+b_3}{b_1+b_2+b_3} & 0 \\ 0 & 0 & -\beta_e\,\dfrac{b_2+b_3}{b_1+b_2+b_3} \end{bmatrix} \tag{27}$$

3.1. Control law definition and closed-loop system dynamics

A suitable control law is necessary for maintaining the solar sail at the L_1-type AEP. Assuming the spacecraft state vector to be measurable, a full-state feedback control law is proposed, that is

$$\boldsymbol{u} = -\mathbb{K}\,\boldsymbol{x} = -\begin{bmatrix} \mathbb{K}_p & \mathbb{K}_d \end{bmatrix}\boldsymbol{x} \tag{28}$$

where $\mathbb{K}_p$ and $\mathbb{K}_d$ are 3×3 sub-matrices of control gains associated with the position and velocity components of the state vector.

The selection of an appropriate set of control gains is not a simple task, since it represents a trade-off solution between system performance and magnitude of the required control inputs. To simplify the design, a linear-quadratic regulator (LQR) is employed, according to which the control law minimizes the functional

$$J \triangleq \frac{1}{2}\int_0^{+\infty} (\boldsymbol{x}^{\mathrm{T}}\mathbb{Q}_x\boldsymbol{x} + \boldsymbol{u}^{\mathrm{T}}\mathbb{Q}_u\boldsymbol{u})\;\mathrm{d}t \tag{29}$$

where $\mathbb{Q}_x \geq 0$ and $\mathbb{Q}_u > 0$ are suitable weighting matrices associated with state and control variables, respectively. Matrices $\{\mathbb{Q}_x, \mathbb{Q}_u\}$ are chosen to be diagonal and the entries of $\mathbb{Q}_u$ have to be significantly larger than those of $\mathbb{Q}_x$ to avoid input saturation problems. The minimization of the J functional of Eq. (29) is obtained by the MATLAB built-in function "`lqr`", which provides the $\mathbb{K}$ matrix.

In general, the solution of an LQR problem corresponds to a matrix $\mathbb{K}$ with all nonzero entries. However, preliminary (and extensive) simulations have shown that the off-diagonal terms of sub-matrices $\mathbb{K}_p$ and $\mathbb{K}_d$ are usually smaller than those on the main diagonal. It is therefore reasonable to set the off-diagonal entries equal to zero and use

$$\mathbb{K}_p = \begin{bmatrix} k_{p1} & 0 & 0 \\ 0 & k_{p2} & 0 \\ 0 & 0 & k_{p3} \end{bmatrix}, \qquad \mathbb{K}_d = \begin{bmatrix} k_{d1} & 0 & 0 \\ 0 & k_{d2} & 0 \\ 0 & 0 & k_{d3} \end{bmatrix} \tag{30}$$

With such a choice, the gains $\{k_{p1},\, k_{d1}\}$, associated with the control variable $\delta\beta$, are used to control the system dynamics along the $\hat{\boldsymbol{i}}$-direction, the gains $\{k_{p2},\, k_{d2}\}$ are associated with ψ and used to control the $\hat{\boldsymbol{j}}$-direction, and finally the gains $\{k_{p3},\, k_{d3}\}$ are involved in the $\hat{\boldsymbol{k}}$-direction dynamics. This significantly simplifies the control law implementation, because each control variable is associated with two state vector components only.

The closed-loop system dynamics is

$$\dot{\boldsymbol{x}} = \mathbb{A}\boldsymbol{x} - \mathbb{B}\mathbb{K}\boldsymbol{x} = (\mathbb{A} - \mathbb{B}\mathbb{K})\boldsymbol{x} = \widetilde{\mathbb{A}}\boldsymbol{x} \tag{31}$$

with $\widetilde{\mathbb{A}} \triangleq \mathbb{A} - \mathbb{B}\mathbb{K}$. The linear stability of the system depends on the eigenvalues of $\widetilde{\mathbb{A}}$, which, in turn, are functions of the control gains $\{k_{pi},\, k_{di}\}$. Unlike the original LQR controller, which is known to give a stable closed-loop system, no a priori guarantee exists on the system stability with a reduced-order controller in the form of Eq. (30). Nevertheless, the suggested procedure gives in practice good results, as will be discussed in the following case study.

3.2. Required control torques evaluation

The desired sail attitude angles θ and ψ must be generated by suitable control torques. To estimate such torques, the angular velocity $\boldsymbol{\omega}$ of the body-fixed reference frame $\mathcal{T}_b$ with respect to an inertial frame is written as

$$\boldsymbol{\omega} = \boldsymbol{\omega}_{\mathrm{bs}} + \boldsymbol{\omega}_{\oplus} \tag{32}$$

where $\boldsymbol{\omega}_{\mathrm{bs}}$ denotes the angular velocity of $\mathcal{T}_b$ with respect to $\mathcal{T}$, and $\boldsymbol{\omega}_{\oplus} = \omega_{\oplus}\hat{\boldsymbol{k}}$ is the angular velocity vector of $\mathcal{T}$ with respect to an inertial frame. Using the rotation matrix of Eq. (20), one obtains

$$[\boldsymbol{\omega}_{\oplus}]_{\mathcal{T}_b} = \mathbb{R}\begin{bmatrix} 0 \\ 0 \\ \omega_{\oplus} \end{bmatrix} = \begin{bmatrix} -\omega_{\oplus}\sin\theta \\ 0 \\ \omega_{\oplus}\cos\theta \end{bmatrix} \tag{33}$$

whereas

$$[\boldsymbol{\omega}_{\mathrm{bs}}]_{\mathcal{T}_b} = \dot{\psi}\mathbb{R}\begin{bmatrix} 0 \\ 0 \\ 1 \end{bmatrix} + \dot{\theta}\begin{bmatrix} \cos\theta & 0 & -\sin\theta \\ 0 & 1 & 0 \\ \sin\theta & 0 & \cos\theta \end{bmatrix}\begin{bmatrix} 0 \\ 1 \\ 0 \end{bmatrix} = \begin{bmatrix} -\dot{\psi}\sin\theta \\ \dot{\theta} \\ \dot{\psi}\cos\theta \end{bmatrix} \tag{34}$$

Substituting Eqs. (33)-(34) into Eq. (32) and assuming small Euler angles, it is found that

$$[\boldsymbol{\omega}]_{\mathcal{T}_b} \simeq \begin{bmatrix} -\theta(\dot{\psi} + \omega_{\oplus}) \\ \dot{\theta} \\ \dot{\psi} + \omega_{\oplus} \end{bmatrix} \triangleq \begin{bmatrix} \omega_1 \\ \omega_2 \\ \omega_3 \end{bmatrix} \tag{35}$$

where $\{\omega_1,\, \omega_2,\, \omega_3\}$ are the components of $\boldsymbol{\omega}$ in $\mathcal{T}_b$.

RCD-based control systems are able to produce small control torques. The sail attitude controlled dynamics may be well approximated by the Euler's equations, viz.

$$I_1\,\dot{\omega_1} + (I_3 - I_2)\,\omega_2\,\omega_3 = M_1 \tag{36}$$

$$I_2\,\dot{\omega_2} + (I_1 - I_3)\,\omega_1\,\omega_3 = M_2 \tag{37}$$

$$I_3\,\dot{\omega_3} + (I_2 - I_1)\,\omega_1\,\omega_2 = M_3 \tag{38}$$

where the subscripts 1, 2 and 3 refer to the principal axes of the body frame $\mathcal{T}_b$. Note that, from the definition of $\mathcal{T}_b$, the torque components M_2 and M_3 can be generated by a suitable RCD activation or deactivation, while M_1 must be provided by PDLCs or by other control actuators; see Fig. 4.

Substituting the angular velocity components given by Eq. (35) into Eqs. (36)–(38), and linearizing for small angles and angular derivatives, yields

$$M_1 = -I_1(\ddot{\psi}\,\theta + \dot{\psi}\,\dot{\theta} + \omega_{\oplus}\dot{\theta}) + (I_3 - I_2)(\dot{\psi} + \omega_{\oplus})\,\dot{\theta} \simeq (I_3 - I_1 - I_2)\omega_{\oplus}\dot{\theta} \tag{39}$$

$$M_2 = I_2\,\ddot{\theta} - (I_1 - I_3)(\dot{\psi} + \omega_{\oplus})^2\,\theta \simeq I_2\,\ddot{\theta} - (I_1 - I_3)\omega_{\oplus}^2\,\theta \tag{40}$$

$$M_3 = I_3\,\ddot{\psi} - (I_2 - I_1)(\dot{\psi} + \omega_{\oplus})\,\dot{\theta}\,\theta \simeq I_3\,\ddot{\psi} \tag{41}$$

which allows the control torques $\{M_1,\, M_2,\, M_3\}$ to be found as functions of the time histories of the Euler angles. Note that three control torques are required to generate the desired time variations of θ and ψ, and to avoid the generation of a sail spinning motion.

4. Case study and numerical simulations

The effectiveness of the proposed control law is now verified by numerical simulations. To that end, a test case scenario is chosen with $l\rho_{\odot_e} = 0.988720$ au, which could guarantee an early-warning time of 1.17 hours, thus improving the performance of NASA's ACE mission [9], of which the warning time is about 1 hour. The position of this L_1-type AEP is shifted towards the Sun of about 189 840 km with respect to the natural equilibrium point L_1. Its maintenance requires a nominal lightness number $\beta_e = 0.0101$, a value close to that of NEA Scout mission [51], which therefore represents the current state-of-the-art of solar sail technology.

The initial conditions are chosen in the vicinity of the L_1-type AEP, with a magnitude of position error of 1000 km (with equal error components in each direction) and a magnitude of velocity error of 1 m/s (again, with equal error components in each direction) [13]. In other terms, the following initial state vector $\boldsymbol{x}_0 \triangleq \boldsymbol{x}(t_0)$ (with $t_0 \triangleq 0$) is considered in the numerical simulations

$$\boldsymbol{x}_0 = [3.859 \times 10^{-6} \quad 3.859 \times 10^{-6} \quad 3.859 \times 10^{-6} \quad 1.938 \times 10^{-5} \quad 1.938 \times 10^{-5} \quad 1.938 \times 10^{-5}]^{\mathrm{T}} \tag{42}$$

This particular choice is based on the assumptions of Folta et al. [52], which are scaled from the Earth-Moon CR3BP to the Sun-[Earth+Moon] CR3BP. Note that other simulated cases with a larger initial bias give similar results, assuming that the initial errors do not increase too much, which would invalidate the linear approximation assumption.

The gains of $\{\mathbb{K}_p,\, \mathbb{K}_d\}$, given by Eq. (30), are obtained from the solution of an LQR problem. First, the coefficients of matrices $\{\mathbb{Q}_x,\, \mathbb{Q}_u\}$ are chosen in accordance with Bryson's rule [53], which suggests assuming both $\mathbb{Q}_x$ and $\mathbb{Q}_u$ to be diagonal matrices, of which the nonzero entries are equal to the inverse square of the maximum desired values of state and control variables, respectively. In particular, a desired position error smaller than 1000 km and a velocity error smaller than 1 m/s (in each direction) are selected, in analogy with Ref. [13] . As for the control variables, a maximum desired value of 5 deg is given for Euler's angles, while the maximum lightness number variation is assumed equal to 1% of the nominal value β_e, a value that is compatible with the current RCD technology [22]. These assumptions are made to ensure that the spacecraft remains in the vicinity of the AEP and that the Euler's angles are small, in order to guarantee the validity of the linear approximation. Therefore, matrices $\{\mathbb{Q}_x,\, \mathbb{Q}_u\}$ are obtained as

$$\mathbb{Q}_x = 10^{10} \times \begin{bmatrix} 2.238\,\mathbb{I} & \mathbb{O} \\ \mathbb{O} & 0.089\,\mathbb{I} \end{bmatrix} \quad , \quad \mathbb{Q}_u = \begin{bmatrix} 9.8 \times 10^7 & 0 & 0 \\ 0 & 130 & 0 \\ 0 & 0 & 130 \end{bmatrix} \tag{43}$$

where $\mathbb{O}$ and $\mathbb{I}$ are 3×3 matrices. Using the proposed procedure, sub-matrices $\{\mathbb{K}_p,\, \mathbb{K}_d\}$ are found to be

$$\mathbb{K}_p = \begin{bmatrix} 22.40 & 0 & 0 \\ 0 & 1.18 \times 10^4 & 0 \\ 0 & 0 & 1.28 \times 10^4 \end{bmatrix} \quad , \quad \mathbb{K}_d = \begin{bmatrix} 7.01 & 0 & 0 \\ 0 & 3.16 \times 10^3 & 0 \\ 0 & 0 & 3.10 \times 10^3 \end{bmatrix} \tag{44}$$

Substituting the control gains of Eq. (44) into Eq. (31), the closed-loop system is found to be stable, and the six eigenvalues of $\widetilde{\mathbb{A}}$ are

$$\lambda_1 = -24.485\,, \quad \lambda_2 = -23.513\,, \quad \lambda_3 = -5.472\,, \quad \lambda_4 = -5.172\,, \quad \lambda_{5,6} = -3.232 \pm 1.591j \tag{45}$$

where j is the imaginary unit. The system dynamics has been simulated by integrating the nonlinear equations of motion (1) for a total flight time of 5 years, using a variable order Adams-Bashforth-Moulton solver scheme [54, 55] with absolute and relative errors of 10^{-12}. The results are reported in Fig. 7 , which shows the time histories of the state variables for $t \leq 100$ days. Note that the system dynamics quickly moves toward the nominal position, which is reached in about 50 days, corresponding to about 14% of the revolution period of the primaries.

Such a spacecraft trajectory requires a maximum lightness variation equal to $\max|\delta\beta| = 0.0220\beta_e$. The corresponding required RCD area can be estimated with the simplified model discussed in Ref. [22].

Assuming a 14 kg-spacecraft equipped with an 86 m^2-sail (values taken from NEA Scout mission [33]), a total RCD area for lightness number control of about 0.35 m^2 is estimated. Note that this value does not take into account the fraction of RCD that are necessary for controlling the sail attitude. Moreover, power generation considerations are neglected in this estimation, since they would require more accurate data on onboard subsystems. Finally, the maximum values (in modulus) of θ and ψ are $\max(|\theta|) \simeq 6.24\,\text{deg}$ and $\max(|\psi|) \simeq 6.08\,\text{deg}$, which are compatible with the previous assumption of small Euler's angles.

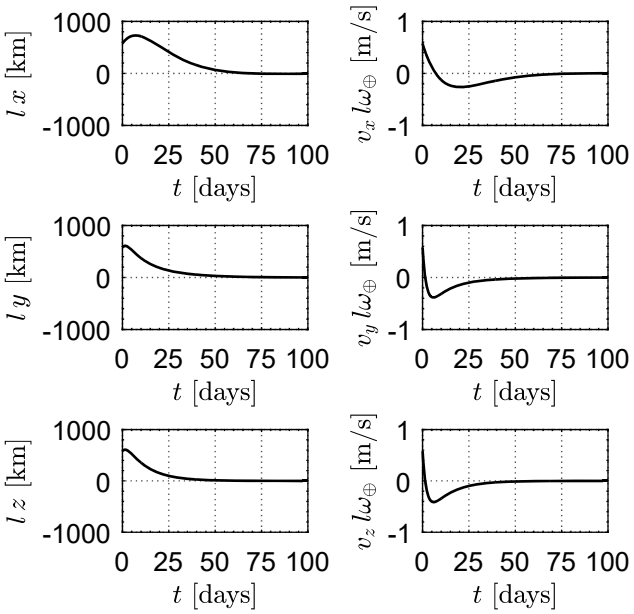

Figure 7: Time histories of the system state variables with gains given by Eq. (44).

Equations (39)–(41) can be used to estimate the magnitude of the required control torques. Because the inertial properties of the solar sail-based spacecraft must be known, some simplifying assumptions are now introduced, that is: i) the sail has a negligible width and an uniform areal density σ; ii) the spacecraft sides are parallel to the axes of $\mathcal{T}_b$; iii) the center-of-mass of the sail coincides with that of the spacecraft main body; iv) the mass of structural elements (booms) is taken into account in the calculation of σ, so it is assumed to be uniformly distributed on the sail surface; v) the spacecraft main body is approximated by a homogeneous parallelepiped with mass m_S. In particular, the first hypothesis is commonly enforced for conventional solar sails [37], the second and the third assumptions are justified by the design of NEA Scout mission [56], while the last two are introduced to overcome the lack of more detailed information. The spacecraft moments of inertia can therefore be written as

$$I_1 = \frac{1}{12}\,(m_S - \sigma A^2)(l_2^2 + l_3^2) + \frac{1}{6}\sigma A^2 \tag{46}$$

$$I_2 = \frac{1}{12}\,(m_S - \sigma A^2)(l_1^2 + l_3^2) + \frac{1}{12}\sigma A^2 \tag{47}$$

$$I_3 = \frac{1}{12}\,(m_S - \sigma A^2)(l_1^2 + l_2^2) + \frac{1}{12}\sigma A^2 \tag{48}$$

where $\{l_1,\, l_2,\, l_3\}$ are the lengths of the three sides of the spacecraft aligned with $\{\hat{\boldsymbol{n}},\, \hat{\boldsymbol{p}},\, \hat{\boldsymbol{q}}\}$. The mass properties of spacecraft NEA Scout [33, 51, 57] are taken as a reference to estimate the moments of inertia, that is, $\beta_e = 0.0101$, $m_S = 14\,\text{kg}$, and $A = 86\,\text{m}^2$. Moreover, since the NEA Scout is a 6U CubeSat, the side lengths are set equal to $\{l_1,\, l_2,\, l_3\} = \{0.3,\, 0.2,\, 0.1\}\,\text{m}$, see Ref. [56]. The total mass of NEA Scout sail (including structural elements) amounts to 3.6 kg [57], and the sail areal density is assumed to be $\sigma = 41.86\,\text{g/m}^2$. As a result, the moments of inertia are estimated to be $\{I_1,\, I_2,\, I_3\} = \{51.64,\, 25.89,\, 25.91\}\,\text{kg}\,\text{m}^2$. The Euler's

equations (39)–(41) are used to quantify the required control torques over a flight time of 5 years, giving $\max\{|M_1|, |M_2|, |M_3|\} = \{1.314, 5.882, 6.058\} \times 10^{-4}$ mN m. Note that the torque components are very small, with M_2 and M_3 that could be generated by covering a small fraction of the sail area near the edges with RCDs devoted to attitude control. Assuming the RCDs to be perfectly opaque in their off state [58], such a fraction amounts to about $0.1\% - 0.2\%$ of the sail total area. In particular, the control torque M_1 could be provided by a small actuator or by PDLC-based control devices.

To further simplify the control law design, the system dynamics has been re-simulated by setting $k_{p2} = k_{p3} = k_{d2} = k_{d3} = 0$ in Eq. (44), while leaving k_{p1} and k_{d1} unchanged. As a result, the only effective control variable is $\delta\beta$, whereas it is assumed that the sail is constantly in a Sun-facing attitude. It may be verified that the eigenvalues of matrix $\widetilde{\mathbb{A}}$ are

$$\lambda_{1,2} = -3.507 \pm 2.571j\,, \quad \lambda_{3,4} = -0.078 \pm 1.332j\,, \quad \lambda_{5,6} = \pm 1.776j \tag{49}$$

showing that the dynamics along the $\hat{\boldsymbol{k}}$-direction is undamped due to the presence of two imaginary eigenvalues. The spacecraft oscillates about the ecliptic plane with an amplitude of about 1800 km, as is shown in Fig. 9. This dynamical behaviour is compatible with the mission requirements (for comparison, ACE mission is tracking a Lissajous orbit with a semimajor axis of 75 000 km and a semiminor axis of 37 500 km, see Ref. [9]). On the other hand, the motion on the ecliptic plane is stable, and the spacecraft moves towards the L_1-type AEP position as is shown in Fig. 8. However, the system dynamics with the simplified control law is significantly slower, and the in-plane distance of the spacecraft from the AEP becomes negligible only after a few years.

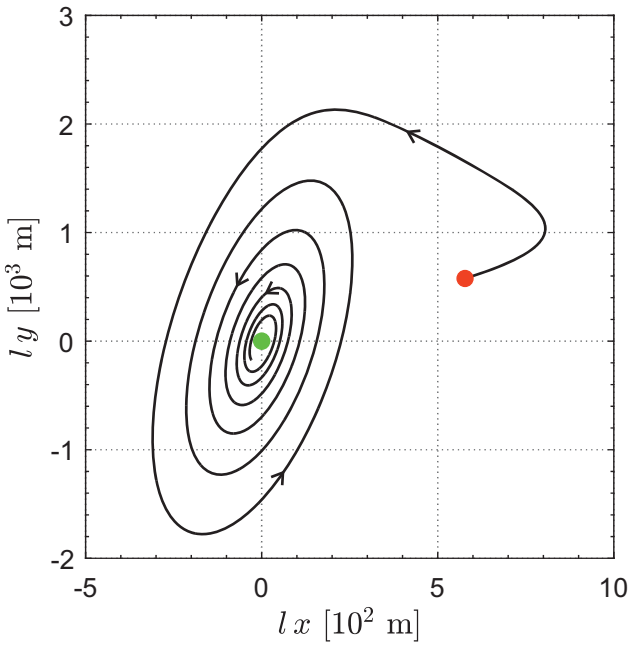

Figure 8: Solar sail trajectory on the ecliptic plane relative to the L_1-type AEP with simplified control law.

Although the possibility of adjusting the propulsive acceleration direction through attitude variation is removed, the dynamical behaviour of the system remains stable. The maximum absolute value of $\delta\beta$ is still about 2.20% of the nominal value, implying that RCDs seem capable of stabilizing the spacecraft in such a mission scenario, as previously stated. These results suggest that a proportional-derivative control in the $\hat{\boldsymbol{i}}$-direction is a good compromise between performance and simplicity for an L_1-type AEP-maintenance control law. The previous considerations are supported by other simulations with different initial conditions (and, consequently, different gains $\mathbb{K}_p$ and $\mathbb{K}_d$), which are not reported here for the sake of conciseness.

The main conclusion that can be deduced is that an accurate control of the sail center-of-mass, which seems possible to obtain by equipping the solar sail with RCDs, is the key factor for guaranteeing an L_1-type

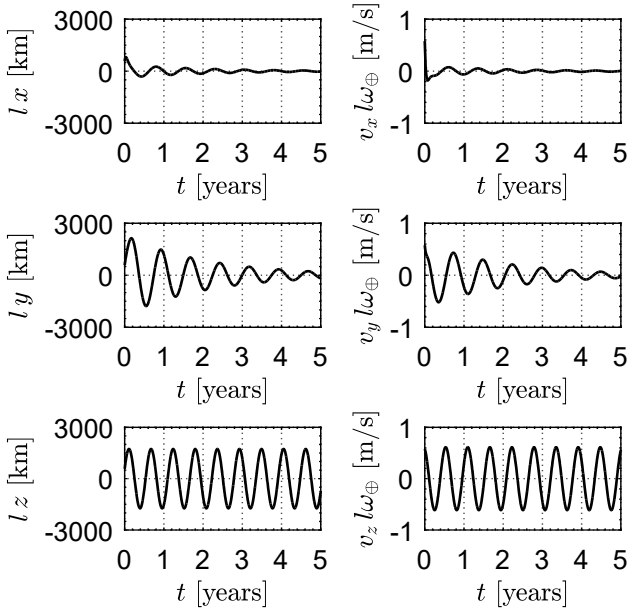

Figure 9: Time histories of the system state variables with simplified control law.

AEP maintenance. If an accurate station keeping is required for mission success, a more complex control law could be implemented, which also accounts for the possibility of adjusting the sail attitude.

5. Conclusions and future perspectives

A preliminary analysis of the possibility of maintaining an L_1-type artificial equilibrium point in the Sun-[Earth+Moon] circular restricted three-body problem by means of a solar sail-based spacecraft has been discussed. A control system capable of adjusting the sail lightness number and the attitude has been assumed, and a full-state control law has been tested, where the control gains are chosen by means of a linear-quadratic regulator approach. The numerical results show that the mission performance mainly depends on the dynamics along the radial direction, and an efficient control may therefore be obtained with a suitable adjustment of the sail lightness number. The latter can be changed by covering a relatively small portion of the sail front surface with reflectivity control devices, manufactured with electrochromic materials. The sail attitude can also be controlled to obtain an asymptotically stable dynamics and a fast convergence toward the equilibrium point. The required torques are small, and can be generated by a set of reflectivity control devices. An extension of the analysis discussed in this work should take into account both the actual orbital eccentricity of the primaries, and the typical ephemeris constraints. In that context, the effect of the electrochromic actuator accuracy should be investigated in a more general mission scenario that involves the generation of non-collinear artificial equilibrium points in the Sun-[Earth+Moon] system.

Funding Sources

This work is supported by the University of Pisa, Progetti di Ricerca di Ateneo (Grant no. PRA-2018-44).

References

[1] V. Szebehely, Theory of orbits: the restricted problem of three bodies, Academic Press, New York, 1967, pp. 8–29.
[2] W. S. Koon, M. W. Lo, J. E. Marsden, S. D. Ross, Dynamical systems, the three-body problem, and space mission design, Springer-Verlag, 2011.
[3] Y. Liang, M. Xu, S. Xu, The classification of cislunar trajectories and its applications in the Earth–Moon system, Astrophysics and Space Science 361 (1) (2016) 1–19 .

[4] Q. Qu, M. Xu, K. Peng, The cislunar low-thrust trajectories via the libration point, Astrophysics and Space Science 362 (5), doi: 10.1007/s10509-017-3075-2.
[5] X. Pan, M. Xu, R. Santos, Trajectory optimization for solar sail in cislunar navigation constellation with minimal lightness number, Aerospace Science and Technology 70 (2017) 559–567, doi: 10.1016/j.ast.2017.08.042.
[6] B. Y. He, H. X. Shen, Solution set calculation of the Sun-perturbed optimal two-impulse trans-lunar orbits using continuation theory, Astrodynamics 4 (1) (2020) 75–86, doi: 10.1007/s42064-020-0069-6.
[7] M. Xu, Y. Liang, X. Fu, Formation flying on quasi-halo orbits in restricted sun-earth/moon system, Aerospace Science and Technology 67 (2017) 118–125, doi: 10.1016/j.ast.2017.03.038.
[8] W. Wang, G. Mengali, A. A. Quarta, J. Yuan, Distributed adaptive synchronization for multiple spacecraft formation flying around lagrange point orbits, Aerospace Science and Technology 74 (2018) 93–103, doi: 10.1016/j.ast.2018.01.007.
[9] E. C. Stone, A. M. Frandsen, R. A. Mewaldt, E. R. Christian, D. Margolies, J. F. Ormes, F. Snow, The Advanced Composition Explorer, Space Science Reviews 86 (1–4) (1998) 1–22 .
[10] A. A. Quarta, G. Mengali, Minimum-time trajectories of electric sail with advanced thrust model, Aerospace Science and Technology 55 (2016) 419–430, doi: 10.1016/j.ast.2016.06.020.
[11] M. Huo, G. Mengali, A. A. Quarta, N. Qi, Electric sail trajectory design with bezier curve-based shaping approach, Aerospace Science and Technology 88 (2019) 126–135, doi: 10.1016/j.ast.2019.03.023.
[12] X. Pan, A. A. Quarta, G. Mengali, M. Xu, Linearized relative motion and proximity control of e-sail-based displaced orbits, Aerospace Science and Technology 99 (105574) (2020) 1–9, doi: 10.1016/j.ast.2019.105574.
[13] L. Niccolai, A. Caruso, A. A. Quarta, G. Mengali, Artificial collinear lagrangian point maintenance with electric solar wind sail, In press. IEEE Transactions on Aerospace and Electronic Systemsdoi: 10.1109/TAES.2020.2990805.
[14] L. Niccolai, A. Anderlini, G. Mengali, A. A. Quarta, Impact of solar wind fluctuations on electric sail mission design, Aerospace Science and Technology 82–83 (2018) 38–45, doi: 10.1016/j.ast.2018.08.032.
[15] G. Mengali, A. A. Quarta, In-orbit repositioning of multiple solar sail spacecraft, Aerospace Science and Technology 12 (7) (2008) 506–514, doi: 10.1016/j.ast.2007.12.003.
[16] S. Gong, H. Baoyin, J. Li, Relative orbit design and control of formation around displaced solar orbits, Aerospace Science and Technology 12 (2) (2008) 195–201, doi: 10.1016/j.ast.2007.05.004.
[17] J. Mu, S. Gong, J. Li, Reflectivity-controlled solar sail formation flying for magnetosphere mission, Aerospace Science and Technology 30 (1) (2013) 339–348, doi: 10.1016/j.ast.2013.09.002.
[18] Y. Song, S. Gong, Solar-sail trajectory design for multiple near-Earth asteroid exploration based on deep neural networks, Aerospace Science and Technology 91 (2019) 28–40, doi: 10.1016/j.ast.2019.04.056.
[19] A. Farrés, J. Heiligers, N. Miguel, Road map to L_4/L_5 with a solar sail, Aerospace Science and Technology 95, doi: 10.1016/j.ast.2019.105458.
[20] C. G. Granqvist, E. Avendano, A. Azens, Electrochromic coatings and devices: survey of some recent advances, Thin Solid Films 442 (1-2) (2003) 201–211, doi: 10.1016/S0040-6090(03)00983-0.
[21] P. M. S. Monk, R. J. Mortimer, D. R. Rosseinsky, Electrochromism: Fundamentals and Applications, Wiley-VCH, 2007.
[22] G. Aliasi, G. Mengali, A. A. Quarta, Artificial Lagrange points for solar sail with electrochromic material panels, Journal of Guidance, Control and Dynamics 36 (5) (2013) 1544–1550, doi: 10.2514/1.58167.
[23] R. Funase, Y. Shirasawa, Y. Mimasu, O. Mori, Y. Tsuda, T. Saiki, J. Kawaguchi, On-orbit verification of fuel-free attitude control system for spinning solar sail utilizing solar radiation pressure, Advances in Space Research 48 (11) (2011) 1740–1746, doi: 10.1016/j.asr.2011.02.022.
[24] S. Firuzi, S. Gong, Refractive sail and its applications in solar sailing, Aerospace Science and Technology 77 (2018) 362–372, doi: 10.1016/j.ast.2018.03.016.
[25] M. Bassetto, A. Caruso, A. A. Quarta, G. Mengali, Optimal steering law of refractive sail, In press. Advances in Space Research doi: 10.1016/j.asr.2019.10.033.
[26] T. Luo, M. Xu, Q. Qu, Design concept for a solar sail with individually controllable elements, Journal of Spacecraft and Rockets 54 (6) (2017) 1389–1397, doi: 10.2514/1.A33775.
[27] H. Baoyin, C. R. McInnes, Solar sail equilibria in the elliptical restricted three-body problem., Journal of Guidance, Control, and Dynamics 29 (3) (2006) 538–543, doi: 10.2514/1.15596.
[28] J. Bookless, C. R. McInnes, Control of lagrange point orbits using solar sail propulsion, Acta Astronautica 62 (2-3) (2008) 159–176, doi: 10.1016/j.actaastro.2006.12.051.
[29] J. D. Biggs, C. R. McInnes, Passive orbit control for space-based geo-engineering, Journal of Guidance, Control and Dynamics 33 (3) (2010) 1017–1020, doi: 10.2514/3.21211.
[30] G. Vulpetti, C. Circi, T. Pino, Coronal mass ejection early-warning mission by solar-photon sailcraft, Acta Astronautica 140 (2017) 113–125, doi: 10.1016/j.actaastro.2017.07.042.
[31] H. Baoyin, C. R. McInnes, Solar sail orbits at artificial sun-Earth libration points, Journal of Guidance, Control, and Dynamics 28 (6) (2005) 1328–1331, doi: 10.2514/1.14598.
[32] J. D. Biggs, C. R. McInnes, T. Waters, Control of solar sail periodic orbits in the elliptic three-body problem, Journal of Guidance, Control, and Dynamics 32 (1) (2009) 318–320, doi: 10.2514/1.38362.
[33] L. McNutt, L. Johnson, P. Kahn, J. Castillo-Rogez, A. Frick, Near-earth asteroid (NEA) scout, in: AIAA SPACE 2014 Conference and Exposition, no. AIAA 2014-4435, San Diego (CA), 4–7 August, 2014.
[34] G. Aliasi, G. Mengali, A. A. Quarta, Artificial equilibrium points for a generalized sail in the circular restricted three-body problem, Celestial Mechanics and Dynamical Astronomy 110 (4) (2011) 343–368, doi: 10.1007/s10569-011-9366-y.
[35] R. H. Battin, An Introduction to the Mathematics and Methods of Astrodynamics, AIAA, 1987, Ch. 8, pp. 371–381.
[36] J. L. Wright, Space Sailing, Gordon and Breach Science Publishers, Philadelphia, PA, 1992.
[37] C. R. McInnes, Solar Sailing: Technology, Dynamics and Mission Applications, Springer-Praxis Series in Space Science and Technology, Springer-Verlag, Berlin, 1999.
[38] G. Mengali, A. A. Quarta, C. Circi, B. Dachwald, Refined solar sail force model with mission application, Journal of Guidance, Control, and Dynamics 30 (2) (2007) 512–520, doi: 10.2514/1.24779.

[39] L. Rios-Reyes, D. J. Scheeres, Generalized model for solar sails, Journal of Spacecraft and Rockets 42 (1) (2005) 182–185, doi: 10.2514/1.9054.
[40] B. Dachwald, G. Mengali, A. A. Quarta, M. Macdonald, Parametric model and optimal control of solar sails with optical degradation, Journal of Guidance, Control, and Dynamics 29 (5) (2006) 1170–1178, doi: 10.2514/1.20313.
[41] B. Dachwald, M. Macdonald, C. R. McInnes, G. Mengali, A. A. Quarta, Impact of optical degradation on solar sail mission performance, Journal of Spacecraft and Rockets 44 (4) (2007) 740–749, doi: 10.2514/1.21432.
[42] L. Niccolai, A. Anderlini, G. Mengali, A. A. Quarta, Effects of optical parameter measurement uncertainties and solar irradiance fluctuations on solar sailing, In press. Advances in Space Research doi: 10.1016/j.asr.2019.11.037.
[43] G. Vulpetti, Fast Solar Sailing: Astrodynamics of Special Sailcraft Trajectories, Springer, Dordrecht, Netherlands, 2013, Ch. 6, pp. 165–254.
[44] D. Zola, C. Circi, G. Vulpetti, S. Scaglione, Photon momentum change of quasi-smooth solar sails, Journal of the Optical Society of America A: Optics and Image Science, and Vision 35 (8) (2018) 1261–1271, doi: 10.1364/JOSAA.35.001261.
[45] A. F. Heaton, A. B. Artusio-Glimpse, An update to NASA reference solar sail thrust model, in: AIAA SPACE 2015 Conference and Exposition, no. AIAA 2015-4506, Pasadena (CA), USA, August 31–September 2, 2015.
[46] A. Heaton, N. Ahmad, K. Miller, Near earth asteroid scout thrust and torque model, in: The 4th International Symposium on Solar Sailing, no. 17055, Kyoto, Japan, 17–20 January, 2017.
[47] L. Niccolai, A. A. Quarta, G. Mengali, Analytical solution of the optimal steering law for non-ideal solar sail, Aerospace Science and Technology 62 (2017) 11–18, doi: 10.1016/j.ast.2016.11.031.
[48] G. Aliasi, G. Mengali, A. A. Quarta, Passive control feasibility of collinear equilibrium points with solar balloons, Journal of Guidance, Control, and Dynamics 35 (5) (2012) 1657–1661, doi: 10.2514/1.57393.
[49] W. Wang, H. Baoyin, G. Mengali, A. A. Quarta, Solar sail cooperative formation flying around L_2-type artificial equilibrium points, Acta Astronautica 169 (2020) 224–239, doi: 10.1016/j.actaastro.2019.10.028.
[50] P. Hughes, Spacecraft Attitude Dynamics, Dover Publications, Mineola, New York, 2004, Ch. 2, pp. 15–20.
[51] J. Pezent, R. Sood, A. Heaton, High-fidelity contingency trajectory design and analysis for NASA's near-earth asteroid (NEA) scout solar sail mission, Acta Astronautica 159 (2019) 385–396, doi: 10.1016/j.actaastro.2019.03.050.
[52] D. C. Folta, T. A. Pavlak, K. C. Howell, M. A. Woodard, D. W. Woodfork, Stationkeeping of lissajous trajectories in the Earth-Moon stystem with applications to ARTEMIS, in: AAS/AIAA Space Flight Mechanics Meeting, San Diego (CA), USA, 2010, pp. 193–208.
[53] A. E. Bryson, Y. C. Ho, Applied Optimal Control, Hemisphere Publishing Corporation, New York (NY), USA, 1975.
[54] L. F. Shampine, M. K. Gordon, Computer Solution of Ordinary Differential Equations: The Initial Value Problem, W. H. Freeman, San Francisco, 1975, Ch. 10.
[55] L. F. Shampine, M. W. Reichelt, The MATLAB ODE suite, SIAM Journal on Scientific Computing 18 (1) (1997) 1–22, doi: 10.1137/S1064827594276424.
[56] J. Orphee, A. F. Heaton, B. Diedrich, B. C. Stiltner, Solar torque management for the Near Earth Asteroid Scout cubesat using center of mass position control, in: AIAA Guidance, Navigation, and Control Conference, Kissimmee (FL), USA, 2018.
[57] D. A. Spencer, L. Johnson, A. C. Long, Solar sailing technology challenges, Aerospace Science and Technology 93, doi: 10.1016/j.ast.2019.07.009.
[58] S. Gong, J. Li, Solar sail halo orbit control using reflectivity control devices, Transactions of the Japan Society for Aeronautical and Space Sciences 57 (5) (2014) 279–288, doi: 10.2322/tjsass.57.279.